Rev. Roum. Sci. Techn.– Électrotechn. et Énerg.
Vol. **63**, *4*, pp. 385–390, Bucarest, 2018

IMPROVEMENT OF THE STARTING CHARACTERISTICS OF AN INDUCTION MOTOR SQUIRREL CAGE BY INSERTION OF FERROMAGNETIC PIECE INSIDE THE SLOTS

ZAKARI MADDI[1], AREZKI DICHE[2], DJAMAL OUZELLAG[1]

Key words: Deep-slot, Induction motor (IM), Ferromagnetic massive piece, Skin effect, Dynamic modeling.

In this paper, a new deep-slot structure of rectangular shape for an induction motor (IM) is proposed. This is obtained by inserting a ferromagnetic massive piece in it. This leads to good starting characteristics of the motor when compared to the conventional shape, *i.e.*, without ferromagnetic massive piece. Two structures of IM were studied: one having the proposed deep-slots and the other presenting conventional deep-slots. To see the influence on the start-up characteristics of the IM, the considered approach is divided in two parts. First, in order to take into account the slot's shape and the skin effect, finite element method is used. The results are compared to those obtained using circuit analysis method. A good agreement is achieved. Aiming to attain global performances, a dynamic modeling of the IM using variable parameters is carried out. The obtained results are presented and discussed.

1. INTRODUCTION

Due to their simplicity of design, high reliability and high efficiency, relatively low cost and easy operation, the IM squirrel cage are largely used as electric actuators. They currently consume more than a half of the overall electrical energy produced in the world. However, these motors are subjected to very high constraints during start-up, the IM develops a relatively low electromagnetic torque in regards to the inrush current, 4 to 8 times the rated current, which causes excessive voltage drops that affects neighboring users and risks damage the motor. In addition, it has significant start-up time inducing a machine overheating. In connection with their wide application, even a minor improvement in the IM characteristics would have a great economic impact [1–3]. The present paper proposes an innovative and powerful solution, in the field of electromechanical systems, using IM exhibiting improved properties at start-up along with optimal characteristics, when operated under controlled variable speed conditions. It consists of inserting a relatively massive ferromagnetic piece in the rotor bar.

The study is conducted in two parts. First, one studied a rectangular deep-slot having ferromagnetic piece, over a frequency operating range, using finite element method (FEM) which allows taking into account the geometrical complexity and the non-uniform repartition of current density (skin effect), in order to determine its resistance and leakage inductance. This is achieved using the FEMM software package [4]. Besides, these parameters were computed for a conventional deep-slot, i.e., without ferromagnetic massive piece. After that, one can obtain the coefficients representing respectively the rate of resistances and leakage reactances which are determined with and without considering the skin effect. In order to check out the validity of our approach, the obtained results are compared to those providing from an analysis circuits method which consists on dividing the slot in several finite resistances and leakage reactances, connected in parallel, thus allowing the calculation of the currents flowing in each branch of this circuit [5]. Finally, a dynamic model of two phase equations of IM (Park transformation), is presented [6]. A study of starting characteristics of the proposed structure (torque and speed), is performed and compared to a conventional model (without skin effect), in order to see the influence of this phenomenon as well as the effect of the ferromagnetic massive piece on the dynamic characteristics of the IM.

2. DEEP RECTANGULAR SLOT MODELING

This type of slot is used to improve the starting conditions of the IM. Due to the sinusoidal supply, the skin effect phenomenon occurs, limiting the magnetic field penetration in the rotor bars. This has a real impact on the rotor resistance and leakage reactance.

3. MODELING WITH FINITE ELEMENT METHOD

The FEM offers the possibility to perform detailed calculations on regions having complex shapes and presenting a magnetic material nonlinearity. It is not surprising that the last decade has seen many proposals for the use of finite element analysis of the IM [7–11]. The alternative approach, in this case, is to compute the current density which varies as a function of frequency, carried out in a rectangular deep-bar (Fig. 1). Therefore the following assumptions are adopted:

- The permeability of the conductor (aluminum) is equal that of vacuum, *i.e.*, $\mu_0 = 4\pi\times 10^{-7}$ H/m.
- The Neumann conditions $\left(\dfrac{\partial \vec{A}}{\partial \vec{n}} = 0\right)$, are applied on the left and right sides of the bar, in order to have the field lines perpendicular to the faces of the bars (to force the flux to cross the border with a 90° degree angle).
- The Dirichlet conditions $\left(\vec{A} = 0\right)$ are applied to the upper and lower sides, to force the flux to be parallel to the boundary.
- The conductivity of the conductor (aluminum), is 34.45×10^{6} S.m^{-1}, within which an electric current of one ampere is imposed.
- The laminated iron conductivity is considered nil and

[1] Université de Bejaia, Faculté de Technologie, Laboratoire de maîtrise des énergies renouvelables, 06000, Algérie, E-mail: zakari.maddi@gmail.com
[2] Université de Tizi-Ouzou, Faculté de Génie Electrique et Informatique, Département d'Electrotechnique, 15000, Algérie

its permeability is infinite, due to its lamination [12].

The bar dimensions are taken from a specification manual of IM 15 kW, $2p = 4$.

A 2D magneto-dynamic equation in terms of the potential vector A, under harmonic hypothesis, is solved using the FEMM software packages. This is done over a frequency range (0 to 50 Hz).

3.1. SIMULATION OF A RECTANGULAR BAR

A structure composed of a single bar instead of the full geometry of the IM which requires considerable time, is presented below. It is simulated in a frequency range in order to calculate the impedance of the bar (taking into consideration the non-uniform distribution of the current density). The simulation results are graphed in Fig. 1. The colors within the bar depict the evolution of the current density, whereas the contours represent the field lines for different frequencies.

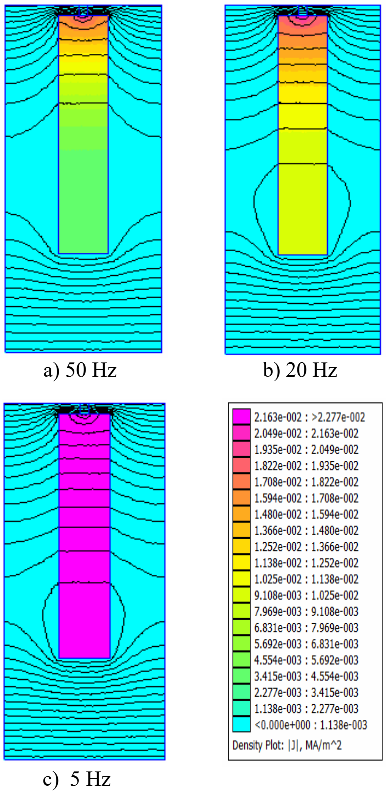

Fig. 1 – Current densities and field lines in a rectangular bar at different

From Fig. 1 one can notice, at start-up conditions that correspond to the frequency of 50 Hz, the non-uniform distribution of the current, assuming higher values near the conductor surface, leading to a high rotor resistance. At the steady state regime (f = 5 Hz), the current is uniformly distributed within the bar, thus reducing its resistance.

4. MODELING USING CIRCUITS METHOD THEORY

Compared to the electromagnetic field theory, this method also takes into account the variation of the rotor impedance caused by the non-uniform repartition of the current density in the slots which is suitable for arbitrary shapes [5]. The bar is divided into n filamental wires. This results for a simple geometric structure (near to a rectangle), in a stair-shaped electrical equivalent circuit composed by resistances and leakage reactance (Fig. 2), where travels a uniform current (nonexistence of skin effect). This means that the penetration depth of the field in the aluminum is lower relative to the radial dimensions of the sub-conductors [13].

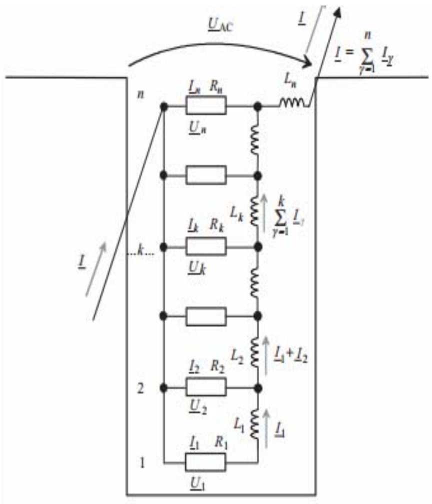

Fig. 2 – Stair-shaped electrical equivalent circuit of a rectangular slot.

The stair-shaped electrical equivalent circuit of figure (2), allows calculating the rotor slot impedance, in its i^{th} elementary conductor. The resistance and leakage reactance of the slot is given by the following equations:

$$\begin{cases} X_\gamma = \omega \times L_\gamma = \omega \times \mu_0 \dfrac{\Delta h_\gamma l}{b_\gamma}, \\ R_\gamma = \rho \dfrac{l}{\Delta h_\gamma b_\gamma} \end{cases} \tag{1}$$

where L_γ – leakage inductance of the sub conductor; ω – rotor angular pulsation; $\lambda_\gamma = \dfrac{\Delta h_\gamma}{b_\gamma}$ – conductibility dispersion coefficient of i^{th} sub-conductor of the slot.

The currents in the sub-conductors are obtained according to the following system of equations:

$$\begin{cases} \dot{\mathbf{I}}_1 = 1 \\ \dot{\mathbf{I}}_2 = \dfrac{R_1}{R_2}\dot{\mathbf{I}}_1 + j\dfrac{\omega L_1}{R_2}\dot{\mathbf{I}}_1 \\ \dot{\mathbf{I}}_3 = \dfrac{R_2}{R_3}\dot{\mathbf{I}}_2 + j\dfrac{\omega L_2}{R_3}\left(\dot{\mathbf{I}}_1 + \dot{\mathbf{I}}_2\right) \\ . \\ . \\ . \\ \dot{\mathbf{I}}_{k+1} = \dfrac{R_k}{R_{k+1}}\dot{\mathbf{I}}_k + j\dfrac{\omega L_k}{R_{k+1}}\left(\dot{\mathbf{I}}_1 + \dot{\mathbf{I}}_2 + ... + \dot{\mathbf{I}}_k\right) \\ \dot{\mathbf{I}}_n = \dfrac{R_{n-1}}{R_n}\dot{\mathbf{I}}_{n-1} + j\dfrac{\omega L_{n-1}}{R_n}\sum\limits_{\gamma=1}^{n-1}\dot{\mathbf{I}}_\gamma \end{cases} \tag{2}$$

In our case the value of the current $\dot{\mathbf{I}}_1$ is equal to 1 A. This way, the total current of the bar is:

$$\dot{I}_b = \sum_{\gamma=1}^{n-1} \dot{I}_\gamma \, . \tag{3}$$

The calculation of the bar resistance R_{be} and the leakage inductance L_{be} taking into account the skin effect, is done using expressions below [14]:

$$R_{be} = \frac{\sum_{\gamma=1}^{n}\left(i_{\gamma}^{2} R_{\gamma}\right)}{i_b^2} \quad (4), \qquad L_{be} = \mu_0 \lambda_{be} l\,, \quad (5)$$

where $\lambda_{be} = \dfrac{\sum_{\gamma=1}^{n}\left(\lambda_{\gamma}\left|\sum_{k=\gamma}^{n} i_k\right|^2\right)}{i_b^2}$. Conductibility dispersion coefficient of the bar taking into account the skin effect.

The coefficients k_r and k_x which allow taking into account the resistance and the leakage inductance variation, are given by the equations (6) and (7):

$$k_r = \frac{R_{be}}{r_0} \quad (6), \qquad k_x = \frac{L_{be}}{L_0}\,, \quad (7)$$

where $r_0 = \rho \dfrac{l}{hb}$ and $L_0 = \mu_0 l \dfrac{\sum_{\gamma=1}^{n}\left(\lambda_{\gamma}\left(\sum_{k=\gamma}^{n} q_k\right)^2\right)}{q_b^2}$ are respectively the resistance and leakage inductance when neglecting the skin effect. While $\sum_{k=\gamma}^{n} q_k$ is the sum of the of the elementary conductors sections.

5. SIMULATION AND RESULTS OF THE TWO METHODS

Simulation results obtained by the two methods presented above (*i.e.* finite element and circuit analysis methods), in case of a rectangular bar are shown in Figs. 3 and 4. They give respectively the evolution of k_r and k_x coefficients in function of the slip.

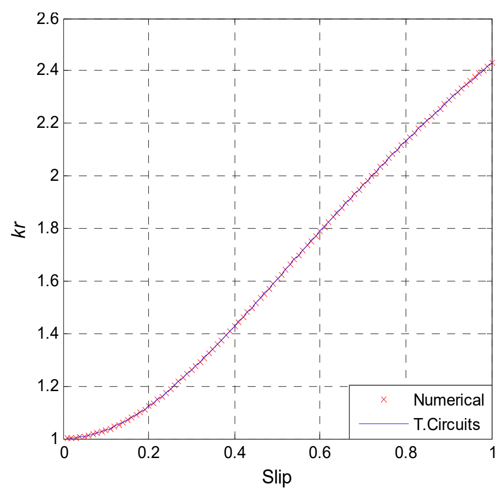

Fig. 3 – Evolution of k_r in function of the slip for rectangular bar.

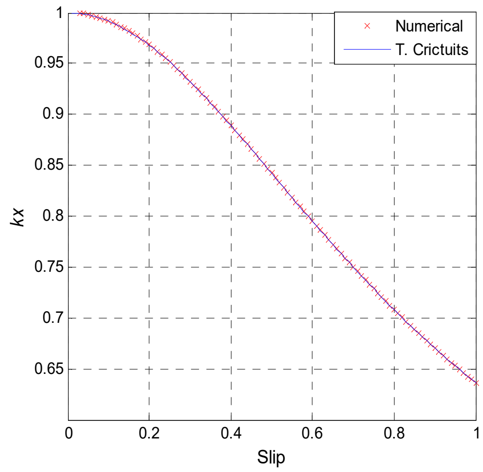

Fig. 4 – Evolution of k_x in function of the slip for rectangular bar.

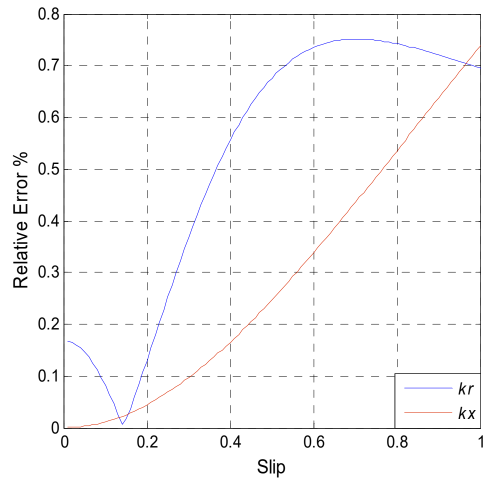

Fig. 5 – Relative error in function of the slip for the two methods.

The error $\text{Error [\%]} = 100 \times \left|\dfrac{k_{nn} - k_{nc}}{k_{nn}}\right|$,

with k_{nn} (k_r or k_x) coefficient for numerical solution;

k_{nc} (k_r or k_x) for circuit analysis solution.

According to Figs. 3 and 4, an exponential increase of the coefficient k_r is noticed, which results in an increase in the resistance, at s = 1 (2.41 times). Conversely, the k_x coefficient decreases which seems as a leakage reactance reduction. At start-up conditions, it is reduced by a factor of 0.6. So the inrush current is reduced and the IM power factor is optimized. Figure (5) shows the maximal relative error, between the results obtained using FEM and circuit analysis method, which doesn't exceed 0.76 %. This confirms the validity of the followed approach.

6. INSERTION OF THE FERROMAGNETIC MASSIVE PIECE

In this part, a more powerful slot structure is proposed. It consists on a rectangular slot having a relatively massive ferromagnetic massive piece inside.

Note that the slot dimensions are set the same as those of the rectangular slot studied before. This piece will act as a junction and let the IM behaves as a double cage one.

Thus, the inrush current will decrease while the torque increases.

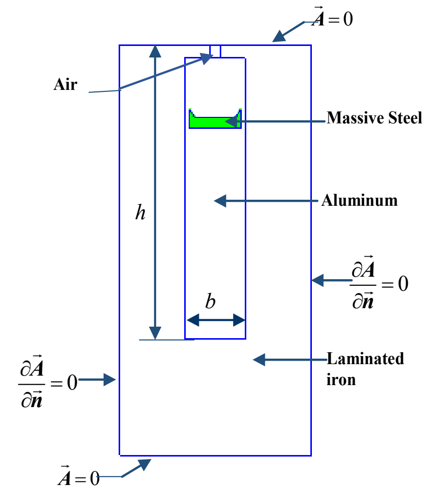

Fig. 6 – Rectangular slot with ferromagnetic piece.

The simulation conditions are set as shown in Fig. 6. The ferromagnetic massive piece presents the conductivity of steel 5.9×10^{6} Sm^{-1}. It is 1.5 mm height and 4.7 mm width.

6.1. RESULTS

A simulation is carried out for the rotor bar with ferromagnetic massive piece, for different frequencies varying from 0 to 50 Hz. It consists on the resolution of the magneto-dynamic equation in terms of potential vector A, in harmonic hypothesis, using finite element method. The obtained results are illustrated in Fig. 7.

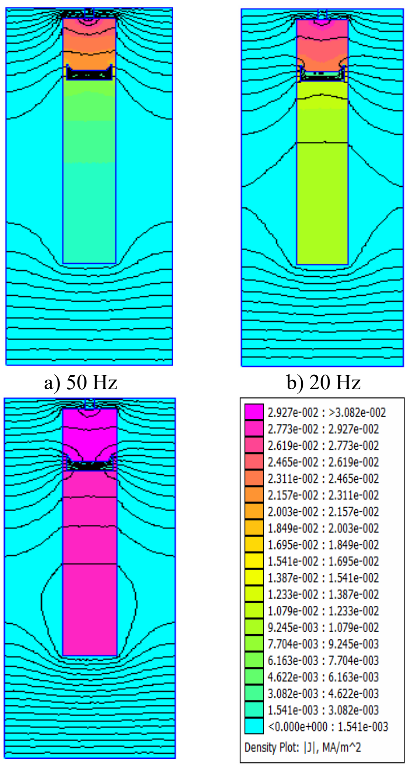

c) 5 Hz

Fig. 7 – Current densities and field lines in a rectangular bar having a ferromagnetic piece at different frequencies.

The evolution of k_r and k_x coefficients obtained with FEM are represented in Figs. 8 and 9.

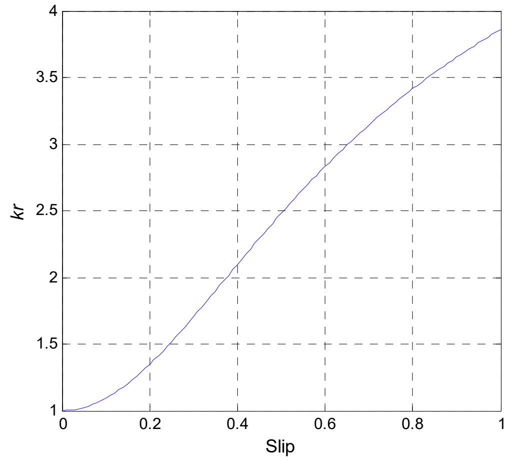

Fig. 8 – Evolution of k_r in function of the slip for rectangular bar with piece by FEM method.

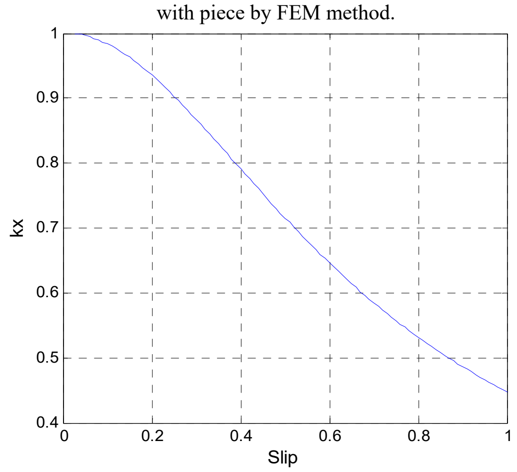

Fig. 9 – Evolution of k_x in function of the slip for rectangular bar with piece by FEM method.

6.2. SIMULATION BY THE METHOD OF THE THEORY OF CIRCUITS

In order to consider the ferromagnetic massive piece effect, the equation (1) is replaced by the following, while the other parameters remain the same as expressed above:

$$\begin{cases} X_\gamma = \omega \times L_\gamma = \omega \times \mu_0 \dfrac{\Delta h_\gamma l}{b_{A\gamma}} \\ R_\gamma = \rho_{e\gamma} \dfrac{l}{\Delta h_\gamma \left(b_{A\gamma} + b_{f\gamma}\right)} \end{cases}, \tag{8}$$

with $\rho_{e\gamma} = \dfrac{\left(b_{A\gamma} + b_{f\gamma}\right)\rho_A \rho_f}{b_{A\gamma}\rho_f + b_{f\gamma}\rho_A}$,

where $b_{A\gamma}$ – aluminum conductor width; $b_{f\gamma}$ – width of the ferromagnetic massive piece; ρ_A – resistivity of aluminum; ρ_f – resistivity of steel.

The simulation results obtained using the theory of circuits method for the two coefficients exhibiting the skin effect, are given in the Figs. 10 and 11.

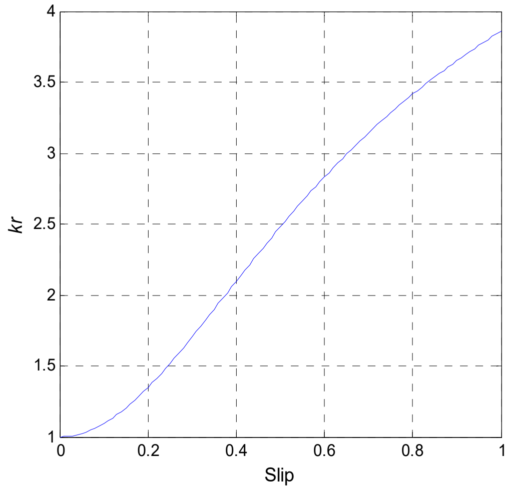

Fig. 10 – Evolution of k_r in function of the slip for rectangular bar with piece by theory of circuits.

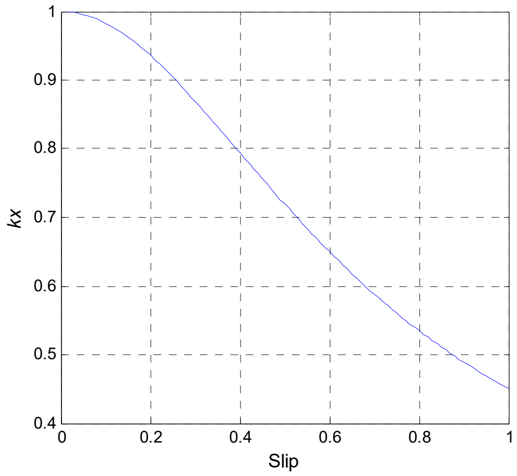

Fig. 11 – Evolution of k_x in function of the slip for rectangular bar with piece by theory of circuits.

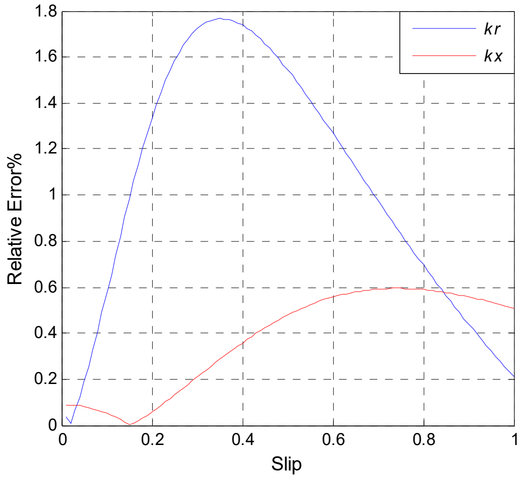

Fig. 12 – Relative error in function of the slip.

Analyzing the relative error between the FEM and theory of circuits obtained results for the two coefficients, k_r and k_x (Fig. 12), where the maximal error is about 1.8 %, one can conclude that a good agreement is achieved. This validates our methodology.

When comparing the results in case of the proposed configuration, *i.e.* a bar with a ferromagnetic piece, to the conventional one, one can see that the parameters are very affected. Indeed, at s=1, k_r grows to 3.8 while k_x decreases to 0.45. Due to the ferromagnetic massive piece, dividing the slot into two parts, the section occupied by the current, decreases. At start-up, the bar working portion is reduced as it can be seen in Fig. 7, resulting in the resistance increasing and thus in the k_r coefficient. In the other hand, as the rotor frequency at start-up, is negligible, this leads to low reactance value, and by the way, in k_x coefficient.

Let notice that in our study, the end-bar effect and the magnetic saturation were neglected.

7. DYNAMIC MODELLING OF IM

The dynamic modeling of IM is presented in the dq reference frame (Park transformation), to take into account the skin effect. The system of equations is given by (9) to (11) [6]:

$$\begin{cases} V_{ds} = R_s i_{ds} + L_s \dfrac{\mathrm{d}i_{ds}}{\mathrm{d}t} + M\dfrac{\mathrm{d}i_{dr}}{\mathrm{d}t} - \omega_s\left(L_s i_{qs} + M i_{qr}\right) \\ V_{qs} = R_s i_{qs} + L_s \dfrac{\mathrm{d}i_{qs}}{\mathrm{d}t} + M\dfrac{\mathrm{d}i_{qr}}{\mathrm{d}t} + \omega_s\left(L_s i_{ds} + M i_{dr}\right) \\ V_{dr} = \left(k_r R'_b + R'_f\right) i_{dr} + \left(\left(k_x l'_b + l'_f\right) + M\right)\dfrac{\mathrm{d}i_{dr}}{\mathrm{d}t} \\ + M\dfrac{\mathrm{d}i_{ds}}{\mathrm{d}t} - \left(\omega_s - \omega_r\right)\left(\left(\left(k_x l'_b + l'_f\right) + M\right) i_{qr} + M i_{qs}\right) \\ V_{qr} = \left(k_r R'_b + R'_f\right) i_{qr} + \left(\left(k_x l'_b + l'_f\right) + M\right)\dfrac{\mathrm{d}i_{qr}}{\mathrm{d}t} \\ + M\dfrac{\mathrm{d}i_{qs}}{\mathrm{d}t} + \left(\omega_s - \omega_r\right)\left(\left(\left(k_x l'_b + l'_f\right) + M\right) i_{dr} + M i_{ds}\right) \end{cases} \tag{9}$$

The stator and rotor flux are connected to the currents, as given by the relations below:

$$\begin{cases} \phi_{ds} = L_s i_{ds} + M i_{dr} \\ \phi_{qs} = L_s i_{qs} + M i_{qr} \\ \phi_{dr} = \left(\left(k_x l'_b + l'_f\right) + M\right) i_{dr} + M i_{ds} \\ \phi_{dr} = \left(\left(k_x l'_b + l'_f\right) + M\right) i_{qr} + M i_{qs} \end{cases}, \tag{10}$$

where R_s – stator phase resistance; L_s – stator cyclic inductance; M – cyclic mutual inductance between the stator and the rotor; R'_b and l'_b – resistance and leakage inductance of the bar portion returned to the stator respectively, traversed by an uniform current; R'_f and l'_f – resistance and leakage inductance of the frontal bar's part returned to the stator respectively.

The electromagnetic torque is given as a function of the rotor flux and stator currents by the following expression:

$$T_e = p\left(\phi_{ds} i_{qs} - \phi_{qs} i_{ds}\right). \tag{11}$$

7.1. STARTING PERFORMANCE OF THE IM

In order to see the improvement due to the proposed deep-slot, on the starting performances of the IM, a whole study is performed. This is achieved by means of a *MATLAB / Simulink*, involving the k_r and k_x coefficients.

The obtained results are depicted in the following Figs.13 and 14.

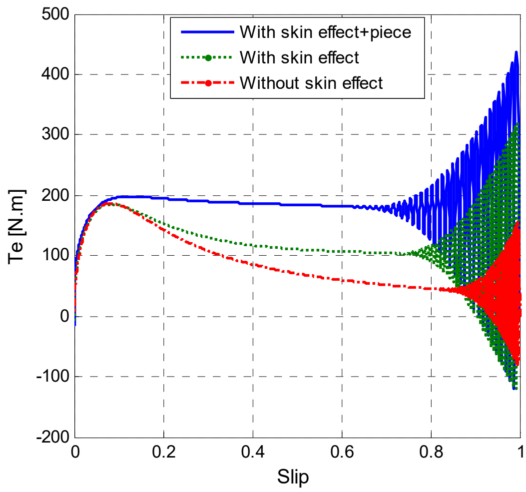

Fig. 13 – Evolution of the electromagnetic torque versus slip.

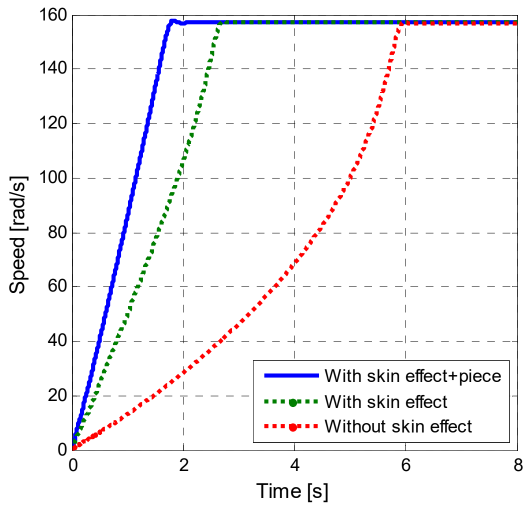

Fig. 14 – Evolution of the speed versus time.

7.2. RESULTS INTERPRETATION

According to the Figs.13 and 14, one can notice that the different start-up characteristics have been improved when using the proposed deep-slot. In fact, the inserted ferromagnetic massive piece acts as a junction and divides the slot into two parts, letting the IM to behave as double-cage one. Indeed, at start-up the current tends to flow in the upper surface of the rotor bar, improving the resistance. This leads to a better starting torque resulting in a good dynamic. Furthermore, in this case, the motor has the advantage to operate at lower speeds since the unstable region is nonexistent (the developed torque is always greater than the resistive torque).

8. **CONCLUSION**

In the present work, a new deep-slot geometry having a ferromagnetic massive piece is proposed. As it can be noticed from the obtained results, the IM has better starting performances, when using the proposed slot.

Generally, the motors presenting such properties occupy an intermediate position between the double-cage IM and solid rotor IM.

According to the methodology presented above, the influence of the ferromagnetic massive piece introduced in the rotor bar, is taken into account by two correction coefficients for the rotor impedance (depending on the frequency, material, shape and dimensions of the slot).

In addition, the used methods, *i.e.* the FEM and theory of circuits, offer the possibility to determine the actual dynamic performances of the IM, as they can be used in a wide range of geometrical structures and desired frequencies, with high accuracy.

Received on December 17, 2016

APPENDIX

Specifications of analyzed motor

Phase, Pole,	3Ph, 4Pole,	Output power	15 kW
Primary voltage	220 V, 50 Hz,	Nominal currant	29.2 A
Stator and rotor diameter	272 mm, 184 mm	Stator/Rotor number slots	48, 36 slots
Core length and	247 mm,	Rated speed	1455 rpm
Height / Width of rotor bar	29.5mm, 5.7mm	Air gap	1mm
R_s	0.302 Ω	X_s	1.754 Ω
R_m	3.622 Ω	X_m	39.21 Ω
R_r'	0.298 Ω	X_r'	1.443 Ω

REFERENCES

1. M. Kostenko, L. Piotrovski., *Machines électriques*, Tome II, Editions Mir, Moscou, Russia, 1979.
2. T. Leuca, G. Cheregi., *A simultaneous induction hardening method of pinions*. Rev. Roum. Sci.Techn. – Électrotechn. et Énerg., **54**, *2*, pp. 157-164, 2009.
3. P. Barret, *Régime transitoire des machines tournantes électriques*, Edition Eyrolles, 1987.
4. D.C. Meeker, *Finite element method magnetics*, User’s Manual.
5. J. Pyrhönen, T. Jokinen, V. Hrabovcovà, *Design of rotating electrical Machines*, Wiley, 2008.
6. Z. Maddi, D. Aouzellag, T. Laddi, *Influence of the skin effect and the form of slot on the starting characteristics of induction motor squirrel cage*, Recent Advances in Mechanics, Mechatronics and Civil, Chemical and Industrial Engineering, pp. 125-129, 2015.
7. A.S. Babb, J.E. Williams, *Circuit analysis method to determination of A-C of machines conductor*, Trans. of AIEE , **70**, pp. 661–666, 1951.
8. A. Simion, L. Livadaru, D. Lucache, E. Romila, *Third order harmonics evaluation by finite element analy analysis of a two-phase induction machine*, Rev. Roum. Sci.Techn.–Électrotechn. et Énerg., **52**,*1*, pp. 23-32, 2007.
9. S. Williamson, M. J. Robinson, *Calculation of cage induction motor equivalent circuit parameters using finite elements*, IEE Proceedings **b**-electric Power Applications, **138**, *5*. IET, 1991.
10. Z. Maddi and D. Aouzellag, *Dynamic Modelling of Induction Motor Squirrel Cage for Different Shapes of Rotor Deep Bars with Estimation of the Skin Effect*, Progress in Electromagnetics Research M, **59**, pp. 147-160, 2017.
11. C. M. Gheorghe, L. M. Melcescu, T. Tudorache, E. Mihai, *Numerical modelling approaches for the analysis of squirrel-cage induction motor,* Rev. Roum. Sci.Techn. – Électrotechn. et Énerg, **61**, *1*, pp. 18-21, 2016.
12. S. Canat, *Contribution à la modélisation dynamique de la machine asynchrone à cage*, Thèse de doctorat de l’Institut National Polytechnique de Toulouse, France, 2006.
13. I. Boldea, S. Nasar, *The induction machine*, Handbook, Boca Raton. FL: CRC, 2002.
14. I. P. Kopilov, *Calculation of the electric machines*, Moscou, Russia, 2002.